Hardware-Based Modulation Strategy to Suppress the Leakage Current for Transformerless Odd-Module Cascaded H-Bridge Inverter in PV System

Pengcheng Zhao, *Student Member, IEEE*, Xiaoqiong He, *Member, IEEE*, Yikai Wang, Chenghao Qiu, and Pengcheng Han, *Student Member, IEEE*

***Abstract*—Transformerless cascaded H-bridge (CHB) grid-connected inverters are widely used in engineering due to its advantages in volume, cost, and efficiency. However, the lack of electrical isolation results in a leakage current loop between the system and earth, creating additional electromagnetic interference and safety issues First, the CHB model with parasitic capacitance is established, and proved that the leakage current of odd-module CHB (OM-CHB) cannot be suppressed solely by modulation. Then, a new hardware-based pulsewidth modulation (HB-PWM) strategy is proposed to suppress the leakage current of OM-CHB. In the proposed strategy, two new redundant states are created by adding two power switches in the intermediate module. These extra switching states are applied to the HB-PWM strategy, which can eliminate the high-frequency component of the sum of parasitic capacitive voltage (SPCV), thus, suppress the leakage current, and available generalizes to CHB with arbitrary odd-module. Finally, the effectiveness of the proposed method is verified by a MATLAB/Simulink simulation model and an experimental prototype with a rated power of 550 W. The experimental results show that the SPCV of the proposed method does not contain high-frequency components, and the value of the leakage current meets the standard of VDE 0126-1-1.**

***Index Terms*—Hardware-based modulation strategy, leakage current suppression, odd-module cascaded h-bridge (OM-CHB), transformerless grid-connected inverters.**

I. Introduction

THE installed capacity and power generation of solar energy has climbed rapidly in successive years, and has played a critical role in new energy grid-connected power generation [1], [2]. In comparison to connecting photovoltaic (PV) power to the grid via grid-frequency transformer or high-frequency transformer, transformerless PV-GCI attracts more and more attention due to its advantages of low cost, small size, light weight, and high efficiency [3], [4]. Nevertheless, a leakage current circuit is formed between the parasitic capacitance of the PV panel, the earth, and the grid due to the lack of electrical isolation [5]. It will cause many issues such as electromagnetic inference, increase of equipment loss and current harmonic distortion, even endangering the safety of personnel [6], [7]. German Standard VDE 0126-1-1 [8] and International Electrotechnical Commission (IEC) 62109-2 [9] specify that PV systems should be disconnected from the point of common coupling within 0.3 s when the root mean square (rms) value over exceeds from 30 mA.

Many advanced suppression methods for the leakage current of classic full-bridge inverters have been proposed, which can be summarized into three ideas. One is based on hardware, such as H5 [10], H6 [11], H7 [12], H10 [13], another is based on software [14], [15], and the last one is comprehensive of hardware and software [16], [17]. The doubly grounded inverters is a new topology that completely eliminates leakage currents by cogrounding the grid neutral with the negative terminal of the PV cell [18]. As a matter of fact, scholars have made a number of research results on doubly grounded inverter topology, such as based on basic chopper circuits [19], quasi-z source circuit [20], H-bridge [21], and so on. However, these methods are only applicable to single-module single-phase or three-phase inverter topology, which cannot be directly adopted in CHB to tackle the leakage current problem.

In PV-GCI systems, since PV modules can provide isolated dc voltage, CHB is more suitable for PV systems than diode clamp converters and flying across capacitors converters [22], [23]. So far, there is rarely publication dealing with the leakage current issue in PV-CHB systems.

As the switching mechanism of the CHB is different from single-module inverters, it is difficult to achieve the desired effect by simply transplanting the existing suppression method. In [24], a mathematical model of the leakage current is established that comprehensively considering various parasitic parameters, but its order is too high to be suitable for CHB. In [25], a simplified model only considering parasitic capacitance parameters is proposed, which is widely used in leakage current research of

Manuscript received 21 May 2023; revised 31 July 2023 and 11 October 2023; accepted 12 November 2023. Date of publication 23 November 2023; date of current version 26 January 2024. This work was supported by the National Natural Science Foundation of China under Grants 52077181 and 2021YFB2601500. Recommended for publication by Associate Editor M. S. ElMoursi. *(Corresponding author: Xiaoqiong He.)*

Pengcheng Zhao, Xiaoqiong He, Yikai Wang, and Pengcheng Han are with the National Rail Transit Electrification and Automation Engineering Technique Research Center, School of Electrical Engineering, Southwest Jiaotong University, Chengdu 611756, China (e-mail: zhaopc@my.swjtu.edu.cn; hexq@swjtu.edu.cn; 1490834741@qq.com; birdhpc@my.swjtu.edu.cn).

Chenghao Qiu is with Tangshan Institute, Southwest Jiaotong University, Chengdu 611756, China (e-mail: qch1726@my.swjtu.edu.cn).

Color versions of one or more figures in this article are available at https://doi.org/10.1109/TPEL.2023.3336073.

Digital Object Identifier 10.1109/TPEL.2023.3336073

CHB. The [22] reveal that the excitation source of CHB leakage current is related to sum of parasitic capacitive voltage (SPCV), which include common-mode voltage (CMV) and differential mode voltage (DMV). A new topology is formed by integrating some structures into CHB, such as H5, H6, and Heric [26], which keeps the CMV of the CHB constant, but the (DMV) still exists. Moghaddam and Iman-Eini [27] designed and placed bidirectional switches on the ac-side of the CHB, which is helpful to keep the CMV constant, but had no effect on the DMV. Wang et al. [28] proposed a modified phase disposition pulsewidth modulation (PWM), which utilizes switching sequence with equal SPCV for each output voltage level. In [29] and [30], the redundant vectors and multicarriers are used to eliminate the leakage current of the two-module CHB, respectively. Unfortunately, the abovementioned methods are suitable for CHB with a fixed number of cascaded modules, cannot be generalized to more modules. wang et al. [31] and Shahabadini and Iman-Eini [32] proposed a new method that suitable for CHB with any even-module, but invalid for OM-CHB. It has been demonstrated that the DMV of the intermediate modules has no contribute to the SPCV, it is infeasible to rely solely on modulation to keep the SPCV of OM-CHB constant [22].

To solve the leakage current of OM-CHB, a method that combining hardware with software has entered the perspective of researchers. By placing common-mode filters on the dc-side and the ac-side of each module, respectively, a filter-based hardware approach is discussed in [25]. Guo and Jia [33] explored a structure that adds filter inductors and capacitors on the ac-side of each module, whose structure is suitable for CHB with any number of cascaded modules, when all the inductors have the same parameters. Shahabadini et al. [34] proposed a Heric-based CHB inverter, in conjunction with utilization of ac-side *LCL* filters, leading to leakage current suppression in individual module, thus, whole system. As it was stated, these methods can eliminate leakage current of CHB with any modules, but excessive extra devices increase the system's cost, losses, and control complexity.

In summary, although many topological and modulation improvements have been proposed to reduce leakage current of CHB inverter, not applicable to OM-CHB. Unfortunately, no paper has been dedicated to the research on leakage current of OM-CHB with arbitrary module. In order to fill this gap, this article proposes a new method to solve the leakage current of OM-CHB with arbitrary modules, which involves adding two power switches in the intermediate module and using the proposed modulation strategy to maintain the SPCV constant, thereby suppressing the leakage current. As shown later, compared with existing solutions, the proposed method can easily be generalized to an arbitrary number of OM-CHB without adding any extra devices. Meanwhile, the effect of leakage current suppression is not influenced by dc-link voltage fluctuation and switching frequency selection. This solution is a candidate to eliminates the leakage current of any OM-CHB.

The rest of this article is organized as follows. In Section II, the CMV-DMV mode of CHB is established and theoretical analysis is given. Section III analyses the proposed topology and modulation strategy in detail, and the general idea of suppressing leakage current is summarized. Simulation and experimental results are reported at Sections IV and V. Finally, Section VI concludes this article.

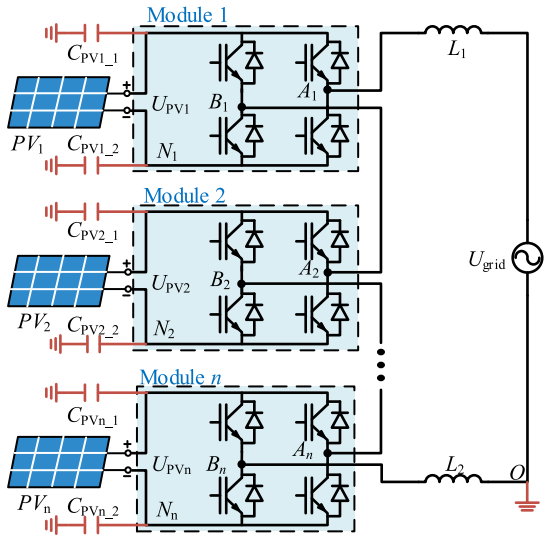

Fig. 1. Topology diagram of conventional single-phase CHB.

II. Analysis of Leakage of Classical CHB

A. Leakage Current Model of Classical CHB

Fig. 1 shows the topology of a single-phase transformerless n-module PV-CHB-GCI with parasitic capacitors. The B-bridge arm of ith module is connected to A-bridge arm of $(i+1)$th module, and total output is connected to single-phase ac grid $U_{\rm grid}$ via two filter inductors L_1, L_2. In Fig. 1, $C_{{\rm PV}i\_k}$ (module index: $i = 12 \ldots n$. k indicates PV panel polarity, "1" for positive, "2" for negative) represents the parasitic capacitance of each module between PV terminals and ground. The $C_{{\rm PV}i\_1}$ and $C_{{\rm PV}i\_2}$ are connected to ground in parallel, thus, the parasitic capacitance of the ith module is $C_{{\rm PV}i} = C_{{\rm PV}i\_1} \| C_{{\rm PV}i\_2}$, when $C_{{\rm PV}i\_1} = C_{{\rm PV}i\_2}$, $C_{{\rm PV}i} = 2C_{{\rm PV}i\_1} = 2C_{{\rm PV}i\_2}$. The value of parasitic capacitance is approximately 60–150 nF/kW [33]. The voltage of dc-link, grid connected current and the ground point are named as "$U_{{\rm PV}i}$," "$i_{\rm g}$," and "O," respectively. The negative terminal of ith module is termed "N_i" as the reference point of output voltage. The midpoints of each H-bridge arm are marked "A_i" and "B_i" as the output terminals for that module.

To simplify the model analysis, it is assumed that all the PV modules have identical parasitic capacitances and voltages of dc-link

$$C_{\rm PV1} = C_{\rm PV2} = \ldots\ldots = C_{\rm PVn} = C_{\rm PV} \tag{1}$$

$$U_{\rm PV1} = U_{\rm PV2} = \ldots\ldots = U_{\rm PVn} = U_{\rm PV}. \tag{2}$$

The switching function S_{ji} is defined as

$$S_{ji} = \begin{cases} 1 & S_{ji}{\rm on} \\ 0 & S_{ji}{\rm off} \end{cases} \quad \begin{pmatrix} {\rm switch\,state\,index} \\ j = a, b \end{pmatrix} \tag{3}$$

where S_{ji} denotes the switching function of bridge arm. The upper and lower power switch states of the same bridge arm are reversed, and S_{ji} coincides with the upper power switch state.

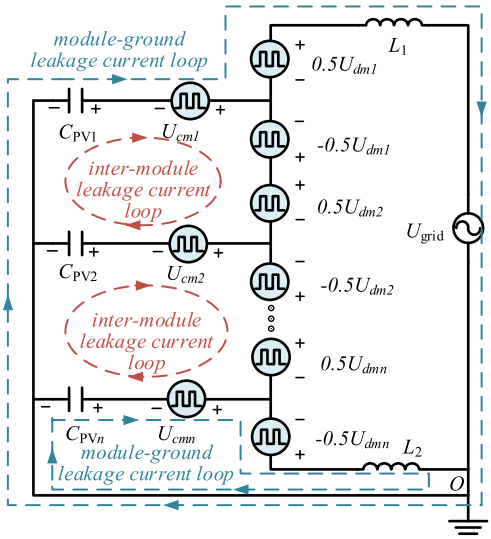

Fig. 2. CMV-DMV equivalent circuit of CHB inverter.

Output voltage of J-bridge arm for i-module can be described as

$$U_{JiNi} = U_{\mathrm{PV}} S_{ji}. \tag{4}$$

The CMV and DMV of a single module H-bridge are defined as follows:

$$\begin{cases} U_{cmi} = \frac{U_{AiNi} + U_{BiNi}}{2} \\ U_{dmi} = U_{AiNi} - U_{BiNi}. \end{cases} \tag{5}$$

Rearranging (5), the voltage of bridge arm can be expressed in terms of CMV and DMV

$$\begin{cases} U_{AiNi} = U_{cmi} + \frac{U_{dmi}}{2} \\ U_{BiNi} = U_{cmi} - \frac{U_{dmi}}{2}. \end{cases} \tag{6}$$

According to (6), the equivalent circuit of Fig. 1 can be derived, as shown in Fig. 2, where U_{Ci} denotes the voltage of the parasitic capacitance for the i-module. i_{lg} is the leakage current of the system, which can be expressed as

$$i_{lg} = C_{\mathrm{PV1}} \frac{\mathrm{d}U_{C1}}{\mathrm{d}t} + C_{\mathrm{PV2}} \frac{\mathrm{d}U_{C2}}{\mathrm{d}t} + \cdots + C_{\mathrm{PV}n} \frac{\mathrm{d}U_{Cn}}{\mathrm{d}t}. \tag{7}$$

Combining (1) and (7), i_{lg} can be rewritten as

$$i_{lg} = C_{\mathrm{PV}} \frac{\mathrm{d}U_{\mathrm{SPCV}}}{\mathrm{d}t} \tag{8}$$

where U_{SPCV} denotes the SPCV of all cascaded module, and $U_{\mathrm{SPCV}} = \sum_{i=1}^{n} U_{Ci}$.

Equation (8) reveals that the excitation source for the leakage current of the CHB is the differential value of U_{SPCV}. Therefore, the idea of suppressing leakage current is to reduce or eliminate the high-frequency components of U_{SPCV}, if U_{SPCV} is constant value, the leakage current does not exist. As it can be seen from Fig. 2, there are two paths of leakage current, one is flowing between intermodule (as shown in the red loop), another is flowing through the grounding point (as shown in the blue loop). The safety standards only limit the leakage current to ground, so this article focuses on the suppression strategy of system leakage current, rather than the leakage current between intermodule.

B. Analysis of Filter Inductance

Generally, the ac-side of CHB is tied to the grid through symmetrical filter (SF) ($L_1 = L_2 \neq 0$) or asymmetrical filter (ASF) ($L_1 \neq 0, L_2 = 0$), and their leakage current characteristics need to be discussed separately.

Applying *Kirchhoff's* voltage law to the structure shown in Fig. 2, the circuit equation can be derived, as shown in

$$\begin{cases} U_{C1} + U_{cm1} - 0.5\left(U_{dm1} + U_{dm2}\right) - U_{cm2} - U_{C2} = 0 \\ U_{C2} + U_{cm2} - 0.5\left(U_{dm2} + U_{dm3}\right) - U_{cm3} - U_{C3} = 0 \\ \vdots \\ U_{C(n-1)} + U_{cm(n-1)} - 0.5\left(U_{dm(n-1)} + U_{dmn}\right) - U_{cmn} \\ -U_{Cn} = 0 \\ U_{Cn} + U_{cmn} - 0.5U_{dmn} + U_{L2} = 0 \\ \sum_{i=1}^{n} U_{dmi} - U_{grid} - U_{L1} - U_{L2} = 0. \end{cases} \tag{9}$$

Analysis of Fig. 2 shows that the difference between SF and ASF lies in the last two circuit equations in (9): SF has the "U_{L2}" term, while ASF does not.

For the convenience of solving, (9) is rewritten in matrix form as (10). As the leakage current is much smaller than the grid current, and the current flowing through L_1 and L_2 is approximately equal, i.e., $U_{L1} = U_{L2}$ in the practical circuit

$$\begin{cases} \boldsymbol{A}_1 \boldsymbol{U}_C^{\mathrm{T}} = \boldsymbol{B}_1 \boldsymbol{U}_{cm}^{\mathrm{T}} + \boldsymbol{C}_1 \boldsymbol{U}_{dm}^{\mathrm{T}} + U_{grid} \boldsymbol{D}_1^{\mathrm{T}} & \mathrm{SF} \\ \boldsymbol{A}_2 \boldsymbol{U}_C^{\mathrm{T}} = \boldsymbol{B}_2 \boldsymbol{U}_{cm}^{\mathrm{T}} + \boldsymbol{C}_2 \boldsymbol{U}_{dm}^{\mathrm{T}} + U_{grid} \boldsymbol{D}_2^{\mathrm{T}} & \mathrm{ASF} \end{cases} \tag{10}$$

where $\boldsymbol{U}_C = [U_{C1} \;\; U_{C2} \;\; \cdots \;\; U_{Cn}]$ denotes the parasitic capacitance voltage matrix, $\boldsymbol{U}_{cm} = [U_{cm1} \;\; U_{cm2} \;\; \cdots \;\; U_{cmn}]$ denotes CMV matrix, and $\boldsymbol{U}_{dm} = [U_{dm1} \;\; U_{dm2} \;\; \cdots \;\; U_{dmn}]$ denotes the DMV matrix. $\boldsymbol{A}_1$, $\boldsymbol{B}_1$, $\boldsymbol{C}_1$, $\boldsymbol{D}_1$ are the coefficients of each excitation source for the SF. $\boldsymbol{A}_2$, $\boldsymbol{B}_2$, $\boldsymbol{C}_2$, $\boldsymbol{D}_2$ are the coefficients of each excitation source for the ASF

$$\boldsymbol{A}_1 = \boldsymbol{A}_2 = \begin{bmatrix} 1 & -1 & 0 & \cdots & 0 \\ 0 & 1 & -1 & \cdots & \\ 0 & 0 & 1 & \cdots & \vdots \\ \vdots & \vdots & \vdots & \ddots & \\ 0 & & \cdots & & 1 \end{bmatrix},$$

$$\boldsymbol{B}_1 = \boldsymbol{B}_2 = \begin{bmatrix} -1 & 1 & 0 & \cdots & 0 \\ 0 & -1 & 1 & \cdots & \\ 0 & 0 & -1 & \cdots & \vdots \\ \vdots & \vdots & \vdots & \ddots & \\ 0 & & \cdots & & -1 \end{bmatrix}$$

$$\boldsymbol{D}_1 = \underbrace{\begin{bmatrix} 0 & \cdots & 0 & -0.5 \end{bmatrix}}_{1\times n}, \boldsymbol{D}_2 = \underbrace{\begin{bmatrix} 0 & 0 & \cdots & 0 \end{bmatrix}}_{1\times n},$$

$$\boldsymbol{C}_1 = \begin{bmatrix} 0.5 & 0.5 & 0 & \cdots & 0 \\ 0 & 0.5 & 0.5 & \cdots & \\ 0 & 0 & 0.5. & \cdots & \vdots \\ \vdots & \vdots & \vdots & \ddots & \\ -0.5 & -0.5 & \cdots & & 0 \end{bmatrix},$$

$$\boldsymbol{C}_2 = \begin{bmatrix} 0.5 & 0.5 & 0 & \cdots & 0 \\ 0 & 0.5 & 0.5 & \cdots & \\ 0 & 0 & 0.5. & \cdots & \vdots \\ \vdots & \vdots & \vdots & \ddots & \\ 0 & 0 & \cdots & & 0.5 \end{bmatrix}.$$

Solving (10) by *Cramer's* law, and get the U_{Ci} of CHB with ASF inductor as

$$U_{Ci\_\mathrm{ASF}} = -U_{cmi} + 0.5U_{dmi} + \sum_{j=i+1}^{n-1} U_{dmj}. \tag{11}$$

The $U_{\mathrm{SPCV\_ASF}}$ can be obtained by performing a cumulative operation on (11). U_{Ci_ASF}, $U_{\mathrm{SPCV\_ASF}}$ denotes the U_{Ci} and U_{SPCV} of CHB with ASF inductor, respectively, as follows:

$$U_{\mathrm{SPCV\_ASF}} = \sum_{i=1}^{n} U_{Ci\_\mathrm{ASF}} = -\sum_{i=1}^{n} U_{cmi} + \sum_{i=1}^{n} (i-0.5)\, U_{dmi}. \tag{12}$$

Similarly, U_{Ci_SF}, $U_{\mathrm{SPCV\_SF}}$ of CHB with SF inductor are shown as

$$\begin{aligned} U_{Ci\_\mathrm{SF}} = & -U_{cmi} + 0.5 \sum_{j=i+1}^{n} U_{dmj} - 0.5 \sum_{j=1}^{i-1} U_{dmj} \\ & + 0.5U_{\mathrm{grid}} \end{aligned} \tag{13}$$

$$\begin{aligned} U_{\mathrm{SPCV\_SF}} = & -\sum_{i=1}^{n} U_{cmi} + 0.5 \sum_{i=1}^{n} (2i-n-1)\, U_{dmi} \\ & + 0.5nU_{\mathrm{grid}}. \end{aligned} \tag{14}$$

From (11)–(14), we can see that the DMV components of $U_{\mathrm{SPCV\_ASF}}$ presenting divergent characteristics, thus, it is impossible to keep constant by modulation.

C. Leakage Current Analysis of OM-CHB

From (14), it can be seen that the DMV components of $U_{\mathrm{SPCV\_SF}}$ is affected by the parity of the number of cascaded modules. If n is even, the DMV components of the ith module and the (n+1-i)th module have similar but opposing sign coefficients, so it is feasible to offsetting effects of DMV by modulation strategies, making $U_{\mathrm{SPCV\_SF}}$ free of high-frequency components. At present, most of modulation strategies for leakage current suppression of even-module CHB are based on this idea.

When n is odd, the DMV coefficient of the (n+1-i)/2-th module is equal to zero, therefore, its DMV components does not contribute to $U_{\mathrm{SPCV\_SF}}$ during output level switching. But the CMV components of the (n+1-i)/2-th module is fluctuating between $+1U_{\mathrm{PV}}$, 0, -1U_{PV}, thus, $U_{\mathrm{SPCV\_SF}}$ cannot kept constant. To sum up, it is unable to eliminate leakage current of OM-CHB by conventional modulation completely.

TABLE I
SWITCHING STATUS IN SYMMETRICAL GROUP

	S_{a1}	S_{b1}	S_{an}	S_{bn}	U_{cm1}+U_{cmn}	U_{dm1}+U_{dmn}
1	1	0	1	0	(0.5+0.5=1)U_{PV}	(1-1=0)U_{PV}
2	0	1	0	1	(0.5+0.5=1)U_{PV}	(-1+1=0)U_{PV}
3	1	1	0	0	(1+0=1)U_{PV}	(0-0=0)U_{PV}
4	0	0	1	1	(0+1=1)U_{PV}	(0-0=0)U_{PV}

TABLE II
OUTPUT VOLTAGE OF GROUP 1

	Module 1	Module n	Output Voltage
1	+U_{PV}	+U_{PV}	+2U_{PV}
2	-U_{PV}	-U_{PV}	-2U_{PV}
3	0	0	0
4	0	0	0

III. PROPOSED TOPOLOGY AND STRATEGY

A. General Idea of OM-CHB Suppress Leakage Current

The $U_{\mathrm{SCV\_SF}}$ of OM-CHB was expanded as (15), which consists of grid voltage, CMV and DMV, among which the grid voltage component mainly contains the fundamental component (50 Hz) and low-frequency harmonics, its effect on the leakage current can be neglected. The CMV and DMV of the CHB are inherently linked by switching function, and should be considered together when designing suppression strategy

$$\begin{aligned} U_{\mathrm{SPCV\_SF}} = & \underbrace{0.5nU_{\mathrm{grid}}}_{\substack{\mathrm{Power-frequency} \\ \mathrm{component}}} \underbrace{-\left[U_{\mathrm{cm1}} + \cdots + U_{\mathrm{cmn}}\right]}_{\mathrm{CMVexcitation\ Source}} \\ & + 0.5 \underbrace{\left[(1-n)\, U_{\mathrm{dm1}} + \cdots + 0 + \cdots + (n-1)\, U_{\mathrm{dmn}}\right]}_{\mathrm{DMVexcitation\ Source}}. \end{aligned} \tag{15}$$

As it can be seen from (15), the DMV components can be eliminated, when the DMV values of the symmetric modules are equal, such as the ith module and the (1+n-i)th module. If the sum of the CMV corresponding to two modules kept constant, the CMV and DMV interference of the symmetric position module is eliminated. At this time, in case the CMV component of the (1+n)/2-th module is a constant value, the $U_{\mathrm{SPCV\_SF}}$ has no high-frequency components.

Based on this idea, the module of OM-CHB is divided into two categories, one is the symmetrical group, another is the middle module of CHB. The symmetrical group contains the ith module and the (1+n-i)th module, the middle module of CHB denotes the (1+n)/2-th module.

From (5), we get switching states that satisfy a constant sum of CMV and DMV in the symmetrical group i as (10-10), (01-01), (11-00), (00-11), and the corresponding power switches are $\mathrm{S}_{\mathrm{a}i}$, $\mathrm{S}_{\mathrm{b}i}$, $\mathrm{S}_{\mathrm{a}(n+1-i)}$, $\mathrm{S}_{\mathrm{b}(n+1-i)}$, respectively. Table I shows the CMV and DMV of symmetrical group 1 (1-th module and nth module), where the sum of CMV is constant $+1U_{\mathrm{PV}}$, and sum of DMV is equal to zero all the time.

Table II shows the output voltage is $+2U_{\mathrm{PV}}$, -2U_{PV},00 in the order, at three even levels, and the sum of multiple module output levels remains even. To ensure smooth switching of output

TABLE III
CMV-DMV CHARACTERISTIC OF H-BRIDGE

	S_a	S_{aN}	S_b	S_{bN}	U_{cm}	U_{dm}	*Output Voltage*
1	1	0	1	0	$+U_{PV}$	0	0
2	1	0	0	1	$+0.5U_{PV}$	$+U_{PV}$	$+U_{PV}$
3	0	1	1	0	$+0.5U_{PV}$	$-U_{PV}$	$-U_{PV}$
4	0	1	0	1	0	0	0

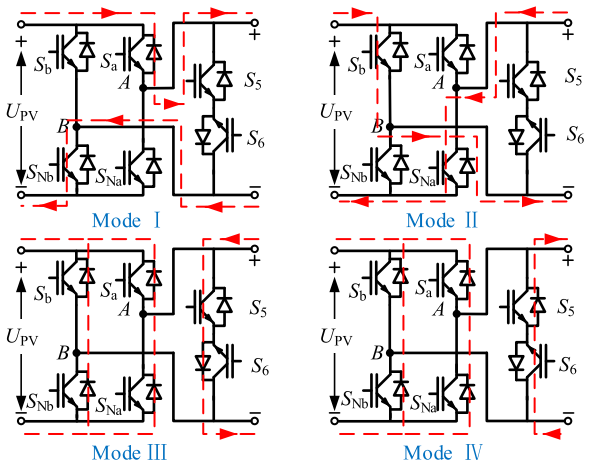

Fig. 3. Operating mode of Heric.

TABLE IV
CMV-DMV CHARACTERISTIC OF INTERMEDIATE MODULE

Mode	S_a/S_{Nb}	S_b/S_{Na}	S_5	S_6	U_{cm}	U_{dm}	Output Voltage
I	1	0	0	0	$0.5U_{PV}$	$+U_{PV}$	$+U_{PV}$
II	0	1	0	0	$0.5U_{PV}$	$-U_{PV}$	$-U_{PV}$
III	0	0	1	0	$0.5U_{PV}$	0	0
IV	0	0	0	1	$0.5U_{PV}$	0	0

levels, the output voltage of middle module of CHB should include three levels of $+U_{PV}$, $-U_{PV}$, and 0.

Table III shows the relationship between CMV-DMV characteristic and output level in H-bridge. The output levels are $+U_{PV}$ and $-U_{PV}$, respectively, when the CMV is constant at $+0.5U_{PV}$, so the intermediate module should also satisfy a new constraint of outputing a zero level when the CMV is $0.5U_{PV}$ as

$$\begin{cases} U_{cm} = \frac{U_{AN}+U_{BN}}{2} = 0.5U_{PV} \\ U_{dm} = U_{AN} - U_{BN} = 0. \end{cases} \tag{16}$$

Solving (16), we get $U_{AN} = U_{BN} = 0.5U_{PV}$.

B. Proposed Topology of Intermediate Module

Combining Table III, it can be seen that conventional H-bridge topology cannot meet this constraint, hence, hardware modification option is considered. Reconstruction structure of H-bridge satisfying the new constraints is shown in [3], the Heric topology is selected due to its fewer extra devices and lower control difficulties.

Fig. 3 shows operation of Heric, and its CMV-DMV characteristic, output levels are shown in Table IV.

Fig. 4 shows the modulation schematic of the proposed topology applied to the n-module. The symmetric groups all use the

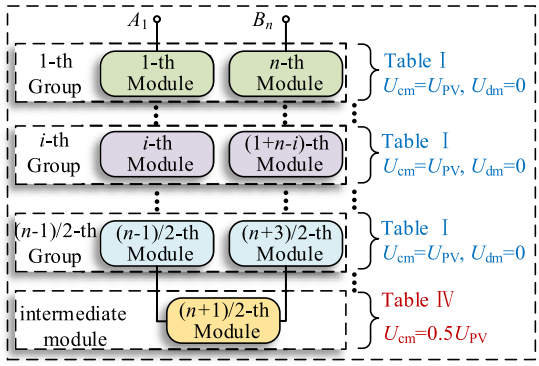

Fig. 4. Proposed topology for n modules.

switching sequences shown in Table I, and the CMV is equal to U_{PV}, the DMV is equal to zero. The intermediate module utilizes the switches sequences shown in Table IV, the CMV is constant at $0.5U_{PV}$. From (15), we can see that the U_{SPCV} is always free of high-frequency components regardless of the increase or decrease in the number of symmetric groups, so the proposed method is suitable for OM-CHB with any modules.

It should be noted that the switching states of two modules within the same group are interrelated, so the output power of each module is consistent. However, the proposed method is not able to freely allocate the power distribution between the symmetric groups and intermediate module, and its effectiveness will be compromised when the PV array is locally shaded. In addition, power distribution is an important performance index of CHB inverter, which has been studied by many scholars [35], but there is no relevant research combining leakage current suppression.

Combining Tables I, IV and Fig. 4, we can easily find that: by the coordination of symmetrical groups and middle module of CHB, smooth switching of the output level while ensuring a constant U_{SPCV_SF} can be achieved. The U_{SPCV_SF} of an n-module CHB can be expressed as

$$U_{SPCV\_SF} = \underbrace{0.5nU_{grid}}_{\substack{\text{Power-frequency} \\ \text{component}}} \underbrace{-0.5nU_{PV}}_{\text{CMV}}. \tag{17}$$

C. HB-PWM Strategy for CHB With Three-Module

To verify the validity of the proposed topology and modulation, leakage current suppression of CHB with three modules is analyzed in this article. The modified topology is shown in Fig. 5, the 1-th module and the 3-th module form symmetrical group 1, 2-th module is modified based on Heric.

Equation (13) can be embodied in the form of three modules as (18), and all of them contain high-frequency switching signals as well as grid voltage signals

$$\begin{cases} U_{C1} = -U_{cm1} + 0.5U_{dm2} + 0.5U_{dm3} + 0.5U_{grid} \\ U_{C2} = -U_{cm2} - 0.5U_{dm1} + 0.5U_{dm3} + 0.5U_{grid} \\ U_{C3} = -U_{cm3} - 0.5U_{dm1} - 0.5U_{dm2} + 0.5U_{grid} \end{cases}. \tag{18}$$

Table V shows the switching status of CHB with three-module, it can be seen that output levels of $+U_{PV}$, $-U_{PV}$, and 0

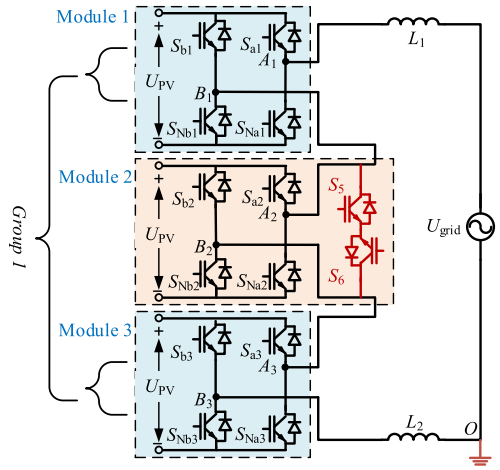

Fig. 5. Proposed Heric-based CHB with three-module.

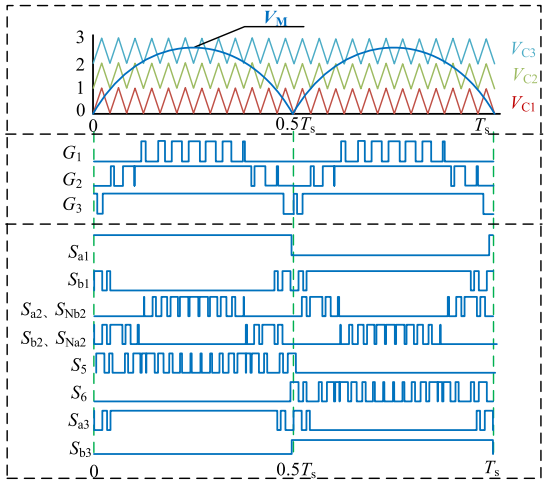

Fig. 6. Switching pattern of the proposed HB-PWM.

TABLE V
SWITCHING STATES OF CHB WITH THREE-MODULE MENTIONED

Output Voltage	S_{a1},S_{b1},S_{a3},S_{b3}, - S_{a2}/S_{Nb2}, S_{b2}/S_{Na2}, S_5 S_6	U_{cm}	U_{dm}	U_{SPCV}
$+3U_{PV}$	1010-10-00	$1.5U_{PV}$	0	$1.5U_{grid}$-$1.5U_{PV}$
$+2U_{PV}$	1010-00-01	$1.5U_{PV}$	0	$1.5U_{grid}$-$1.5U_{PV}$
	1010-01-00	**$1.5U_{PV}$**	**0**	**$1.5U_{grid}$-$1.5U_{PV}$**
$+1U_{PV}$	1100-10-00	$1.5U_{PV}$	0	$1.5U_{grid}$-$1.5U_{PV}$
	0011-10-00	$1.5U_{PV}$	0	$1.5U_{grid}$-$1.5U_{PV}$
	1100-00-10	**$1.5U_{PV}$**	**0**	**$1.5U_{grid}$-$1.5U_{PV}$**
0	0011-00-01	$1.5U_{PV}$	0	$1.5U_{grid}$-$1.5U_{PV}$
	1100-01-00	$1.5U_{PV}$	0	$1.5U_{grid}$-$1.5U_{PV}$
$-1U_{PV}$	0011-01-00	$1.5U_{PV}$	0	$1.5U_{grid}$-$1.5U_{PV}$
	0101-10-00	**$1.5U_{PV}$**	**0**	**$1.5U_{grid}$-$1.5U_{PV}$**
$-2U_{PV}$	0101-00-10	$1.5U_{PV}$	0	$1.5U_{grid}$-$1.5U_{PV}$
$-3U_{PV}$	0101-01-00	$1.5U_{PV}$	0	$1.5U_{grid}$-$1.5U_{PV}$

contains multiple switching states. For example, the $+U_{PV}$ can be obtained by $+2U_{PV}$ of 1-th group and -1U_{PV} of 2-th module, or 0 of 1-th group and $+1U_{PV}$ of 2-th module. The bold parts in Table V are the switching states to be selected in this article.

Conventional phase disposition PWM (PD-PWM) and phase shifted PWM (PS-PWM) technology can achieve CHB grid connection easily, but they cannot generate the switching logic shown in Table V, and have almost no effect on leakage current suppression. To overcome this issue, A new HB-PWM strategy is proposed.

In Fig. 6, the triangular carrier waveforms $V_{c1\text{-}3}$ are in phase and all have an amplitude of 1, and $V_{c2} = V_{c1}+1$ and $V_{c3} = V_{c2}+1$. Assume V_{ref} is the reference signal shown in (19), where M is the modulation index, $M\in(01)$, ω denotes angular-frequency of grid. To reduce the number of carriers, the modulation signal V_M by calculating the absolute value of the V_{ref}

$$V_{ref} = 3M\sin(\omega t). \tag{19}$$

The V_{sgn} reference signal is defined as

$$V_{sgn} = \mathrm{sgn}\,(V_{ref}) = \begin{cases} 1 & V_{ref} > 0 \\ 0 & V_{ref} \le 0 \end{cases}. \tag{20}$$

The preprocessed signal G_1, G_2, and G_3 are obtained by comparing V_m with the carriers V_{c1}, V_{c2}, and V_{c3}, respectively. Switching drive signal of each module as follow:

$$S_{a1} = \overline{S_{b3}} = V_{sgn} \tag{21a}$$

$$S_{b1} = \overline{G_1}V_{sgn} + G_1\overline{V_{sgn}} \tag{21b}$$

$$\begin{aligned} S_{a2} &= S_{N\_b2} \\ &= G_3V_{sgn} + (G_1\,[0 \le V_M \le V_{C1}] \\ &\quad +\overline{G_2}\,[1 \le V_M \le 2])\,\overline{V_{sgn}} \end{aligned} \tag{21c}$$

$$\begin{aligned} S_{b2} &= S_{N\_a2} \\ &= G_1\,[0 \le V_M \le V_{C1}]\,V_{sgn} + \left(G_3 + \overline{G_2}\,[1 \le V_M \le 2]\right)\overline{V_{sgn}} \end{aligned} \tag{21d}$$

$$S_5 = \overline{S_{a2} + S_{b2}}V_{sgn} \tag{21e}$$

$$S_6 = \overline{S_{a2} + S_{b2}V_{sgn}} \tag{21f}$$

$$S_{a3} = G_1V_{sgn} + \overline{G_1V_{sgn}}. \tag{21g}$$

From (13) and Table V, the U_{C1}, U_{C2}, and U_{C3} of CHB with three-module can be derived as (22). And we can see that U_{C2} and "U_{C1}+U_{C3}" contain only the dc component and the mains voltage component, thus, the leakage current is suppressed effectively

$$\begin{cases} U_{C2} = -0.5U_{PV} + 0.5U_{grid} \\ U_{C1} + U_{C3} = -U_{PV} + U_{grid} \end{cases}. \tag{22}$$

Similarly, the switching states of CHB with five-module can be derived, as shown in Table VI, and the switching states of CHB with more odd-numbered can also be obtained by the same way, which will not be repeated here.

IV. SIMULATION STUDY

In this section, the proposed method for OM-CHB leakage current suppression is verified in MATLAB/Simulink, and the results are compared with the PD-PWM and PS-PWM. The parameters in simulation include: dc-link voltage ($U_{PV\,i}$) of 30 V

TABLE VI
SWITCHING STATES OF CHB WITH FIVEMODULE

Output Voltage	S_{a1}~S_{b2},-S_{a4}~S_{b5}	S_{a3}/S_{Nb3}, S_{b3}/S_{Na3}, -S_5,S_6	U_{SPCV}
+5U_{PV}	1010-1010	10-00	2.5(U_{grid}-U_{PV})
+4U_{PV}	1010-1010	00-01	2.5(U_{grid}-U_{PV})
+3U_{PV}	1010-1010	01-00	2.5(U_{grid}-U_{PV})
+2U_{PV}	1011-0010	00-01	2.5(U_{grid}-U_{PV})
+1U_{PV}	1011-0010	01-00	2.5(U_{grid}-U_{PV})
0U_{PV}	1111-0000	00-01	2.5(U_{grid}-U_{PV})
-1U_{PV}	0100-1101	10-00	2.5(U_{grid}-U_{PV})
-2U_{PV}	0100-1101	00-10	2.5(U_{grid}-U_{PV})
-3U_{PV}	0101-0101	10-00	2.5(U_{grid}-U_{PV})
-4U_{PV}	0101-0101	00-10	2.5(U_{grid}-U_{PV})
-5U_{PV}	0101-0101	01-00	2.5(U_{grid}-U_{PV})

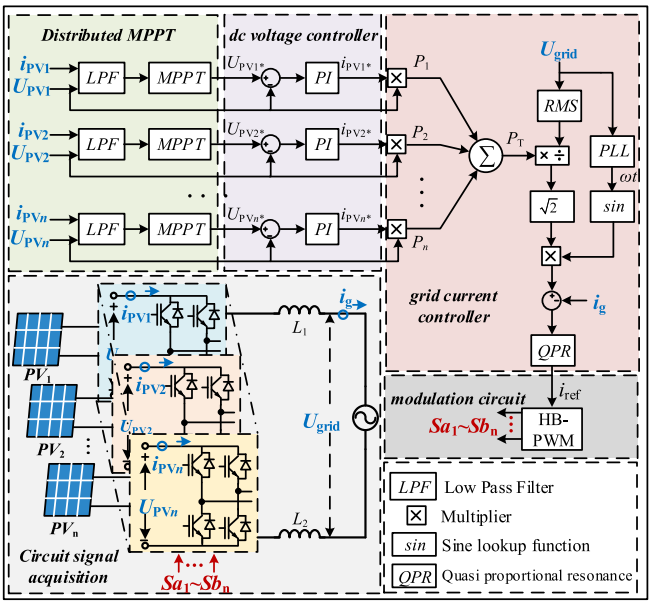

Fig. 7. Control block diagram of CHB-based PV system.

at each module, the parasitic capacitance ($C_{PV\,i}$) of 50 nF, the grid voltage amplitude (U_{grid}) of 80 V and 50 Hz, the filtering inductance $L_1 = L_2 = 2$ mH, the switching frequency of 2 kHz, and grid current amplitude (i_g) of 5 A.

Fig. 7 demonstrates the utilized control system for the grid-connected CHB inverter in this article, which is made of four parts: 1) the distributed maximum power point tracking (MPPT) to obtain the maximum generation power of each PV array, 2) a dc voltage controller to control the dc-link voltage with a proportional integral (PI) regulator, 3) a grid current controller to generate the grid connected current reference signals, and 4) the modulation circuit, in which the proposed modulation approach is used.

A. Simulation Results of HB-PWM and Traditional Strategies

Fig. 8 shows the simulation waveform of HB-PWM. Fig. 8(a) shows that the seven-level waveform of total output voltage can be achieved. Fig. 8(b) shows the grid voltage and grid current, which are highly sinusoidal and in cophase. The total harmonic distortion (THD) of the grid current is 0.52%, which meets the IEEE Std.929-2000 standard of 5%.

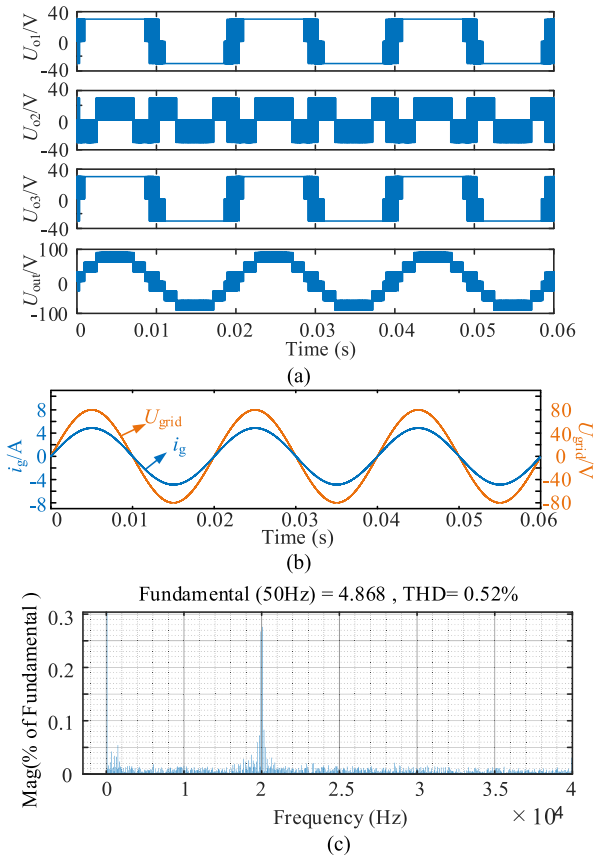

Fig. 8. HB-PWM simulation waveform. (a) Output voltage of each module and total output voltage. (b) Grid voltage and grid current. (c) THD of grid current.

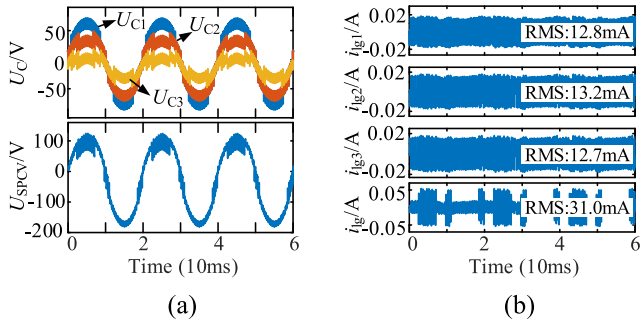

Fig. 9. Simulation results of PD-PWM. (a) U_{Ci} and U_{SPCV}. (b) Leakage current $i_{lg\,i}$ and i_{lg}.

Figs. 9–11 show the simulation results of PD-PWM, PS-PWM, and HB-PWM, respectively. Analyzing of Figs. 9 and 10, we can find that the U_{Ci} and U_{SPCV} of the PD-PWM and PS-PWM contains complex high-frequency components, and rms value of 31.0 mA and 36.0 mA for the leakage current, respectively, which does not meet the standard's requirements.

According to Fig. 11(a), U_{C2} is a sinusoidal waveform with superimposed dc components, without any high-frequency components. Conversely, the U_{C1} and U_{C3} waveform contains complex high-frequency components, but offset each other when

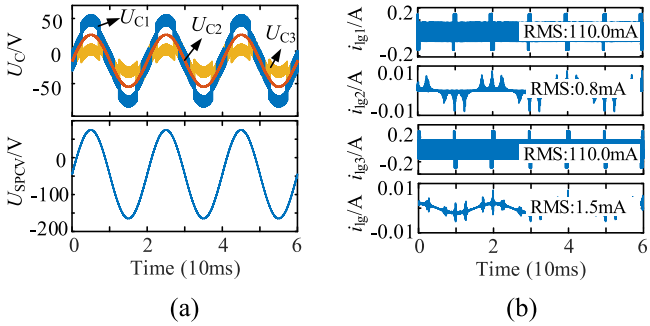

Fig. 11. Simulation results of HB-PWM. (a) U_{Ci} and U_{SPCV}. (b) Leakage current $i_{\mathrm{lg}i}$ and i_{lg}.

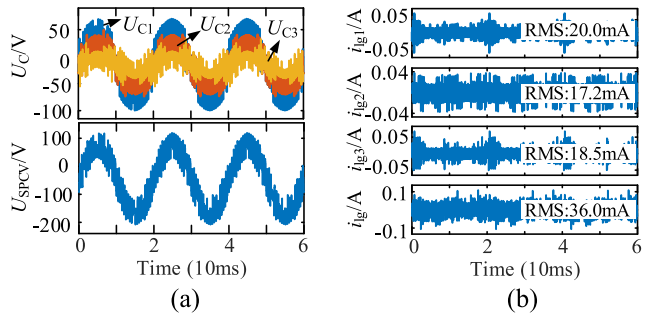

Fig. 10. Simulation results of PS-PWM. (a) U_{Ci} and U_{SPCV}. (b) Leakage current $i_{\mathrm{lg}i}$ and i_{lg}.

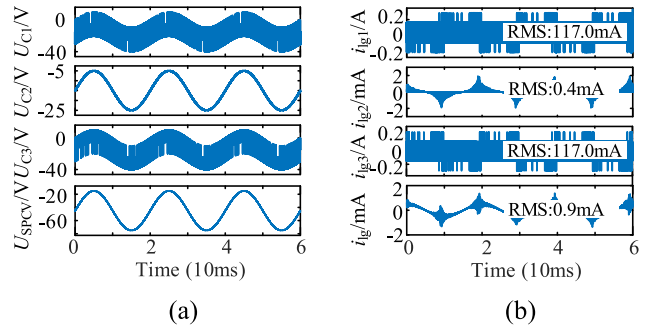

Fig. 12. Simulation results of HB-PWM at modulation index of M_2. (a) U_{Ci} and U_{SPCV}. (b) $i_{\mathrm{lg}i}$ and i_{lg}.

added together. Thus, the U_{SPCV} is an ideal sinusoidal waveform. And the leakage current of each module has a similar relationship, as shown in Fig. 11(b). The rms value of leakage current i_{lg} is 1.5 mA, which satisfies the VDE 0126-1-1 and IEC 62109-2.

B. Simulation Results of HB-PWM at all Modulation Index

To further verify that the proposed approach can suppress leakage current at all modulation index, the modulation indexes of CHB with three-module is divided into $M_1 \in (01/3)$, $M_2 \in (1/32/3)$, $M_3 \in (2/31)$. The modulation index of Fig. 10 is 0.88, the next step research will focus on M_1 and M_2, and set the grid voltage amplitude to 20 V, 50 V, respectively, when the modulation index is M_1 and M_2.

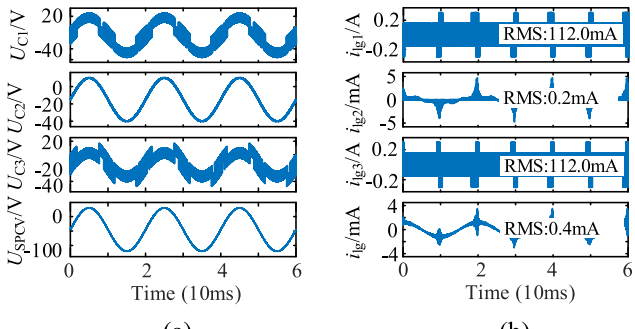

Fig. 13. Simulation results of HB-PWM at modulation index of M_1. (a) U_{Ci} and U_{SPCV}. (b) $i_{\mathrm{lg}i}$ and i_{lg}.

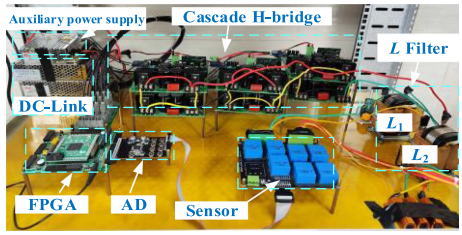

Fig. 14. Experiment prototype of CHB with three-module.

TABLE VII
PARAMETERS OF EXPERIMENTAL PROTOTYPE

Parameters	Values
Number of H-bridge cells	3
Dc-link Voltage	60 Vdc for each module
Grid Voltage	Single-phase AC grid 50Hz 110 V / 70 V /35 V(rms)
Parasitic Capacitance	50 nF/module
Filter inductor	2 mH*2
Switch frequency	2 kHz
Grid current	5 A(rms)
Rated power	550 W

Figs. 12 and 13 show simulation results of HB-PWM at grid voltage amplitude of 50 V and 20 V separately. As shown in Figs. 12 and 13, the waveform characteristics of the U_{Ci} and $i_{\mathrm{lg}i}$ of each module are consistent with Fig. 11, and the rms value of the leakage current are 0.9 mA and 0.4 mA when grid voltage amplitude at 50 V and 20 V, respectively.

V. Experimental Result and Analysis

A prototype shown in Fig. 14 has been designed, and the results are presented in this section. The prototype consists of three identical H-bridge power boards, symmetrical filter $L_{1,2}$, dc power source (simulate PV array), and programmable ac power supply. The master controller is an FPGA for the implementation of modulation and closed loop quasi-proportional resonance current control. The main parameters of this platformare listed in Table VII.

A. Experiment Results of HB-PWM and Traditional Strategies

Figs. 15 –18 show the experimental results of PD-PWM, PS-PWM, and HB-PWM separately. Fig. 15 illustrate that the output

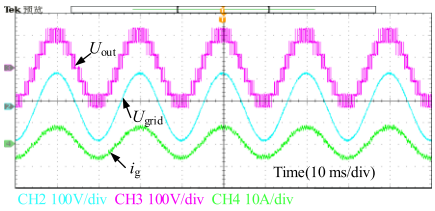

Fig. 15. Experimental results of HB-PWM, the wave of output voltage U_{out}, grid voltage U_{grid}, and grid current i_{g}.

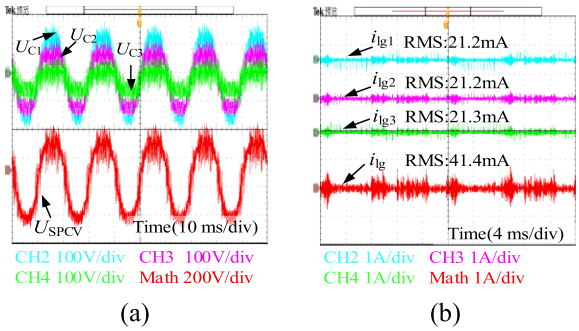

Fig. 16. Experimental results of PD-PWM. (a) $U_{\mathrm{C}i}$ and U_{SPCV}. (b) $i_{\mathrm{lg}i}$ and i_{lg}.

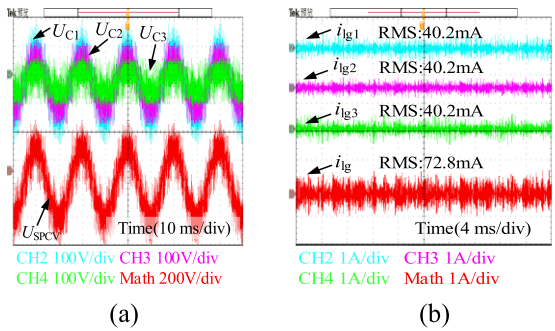

Fig. 17. Experimental results of PS-PWM. (a) $U_{\mathrm{C}i}$ and U_{SPCV}. (b) $i_{\mathrm{lg}i}$ and i_{lg}.

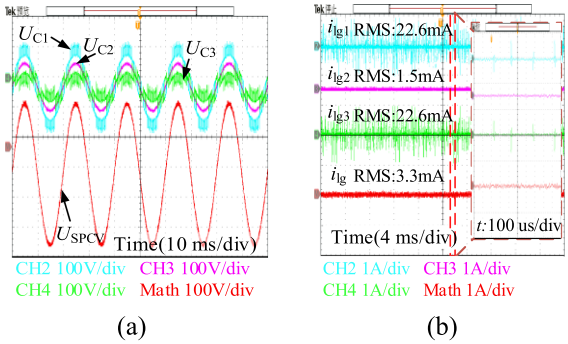

Fig. 18. Experimental results of HB-PWM. (a) $U_{\mathrm{C}i}$ and U_{SPCV}. (b) $i_{\mathrm{lg}i}$ and i_{lg}.

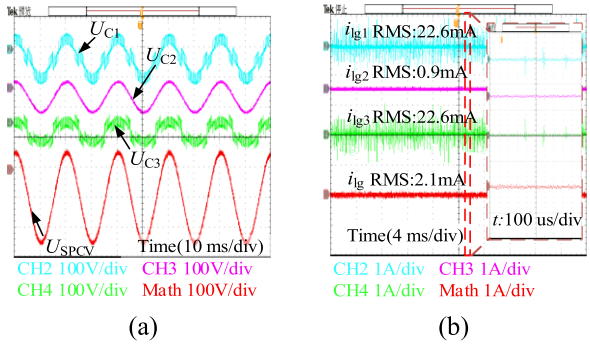

Fig. 19. Experimental results of HB-PWM at grid voltage of 70 Vrms. (a) $U_{\mathrm{C}i}$ and U_{SPCV}. (b) $i_{\mathrm{lg}i}$ and i_{lg}.

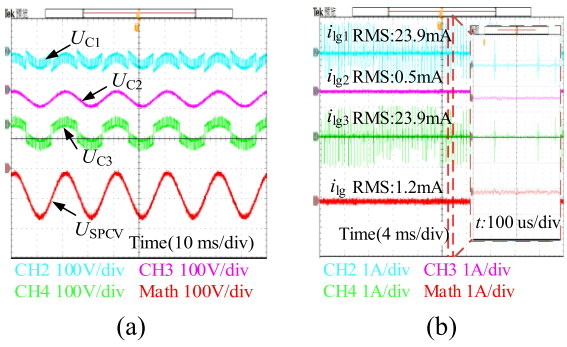

Fig. 20. Experimental results of HB-PWM at grid voltage of 35 Vrms. (a) $U_{\mathrm{C}i}$ and U_{SPCV}. (b) $i_{\mathrm{lg}i}$ and i_{lg}.

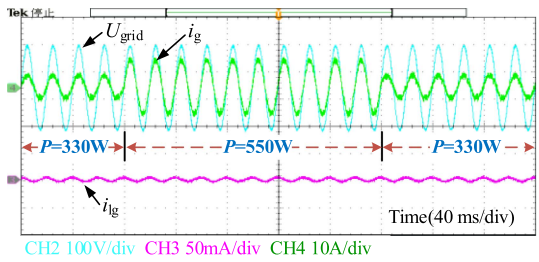

Fig. 21. Effect of active power change on the leakage current.

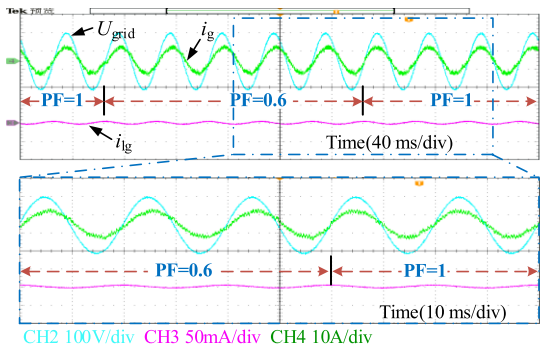

Fig. 22. Effect of reactive power injection on the leakage current.

voltages of inverter have seven-level voltage steps and the grid currents are well sinusoidal. In subplot(a) of Figs. 16 and 17, the U_{Ci} and U_{SPCV} of PD-PWM, PS-PWM contains complex high-frequency components, which leading to a high leakage current with rms value of 41.4 mA and 72.8 mA, and cannot meet the VDE0126-1-1 standard. From Fig. 18(a), it can be observed that the waveform burr of U_{C1} and U_{C3} is symmetrical about U_{C2}, the U_{C2} and U_{SPCV} are almost sinusoidal, and total leakage current is almost zero (3.3 mA), far below the safety standards, coinciding with the analysis of (22).

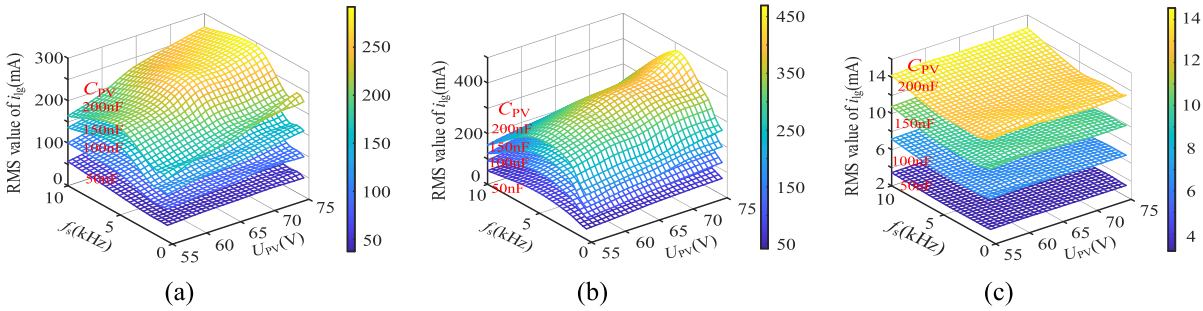

Fig. 23. Effects of switching frequency, parasitic capacitance value, and DC-link voltage on leakage current. (a) PD-PWM. (b) PS-PWM. (c) HB-PWM.

B. Dynamic Performance of the Proposed HB-PWM

Figs. 19 and 20 show the experimental results of HB-PWM at grid voltage of 70 Vrms and 35 Vrms separately. The results indicate that the proposed strategy has an excellent performance of grid connection at different modulation index, and the variation trend of parasitic capacitor voltage in each module is also agree with Fig. 18. Subplot(b) of Figs. 19 and 20 illustrate the rms value of total leakage current of 2.1 mA and 1.2 mA in succession, the root cause is that the decrease in low-frequency leakage current caused by the grid voltage reduction.

Figs. 21 and 22 show the experimental results of the proposed HB-PWM strategy for active power variations and different reactive power injection, respectively. As can be seen, the leakage current waveforms are free from the influence of active power variations or reactive power injection, which shows the excellent dynamic performance of the proposed method.

C. Leakage Current for Different Circuit Parameters

From Fig. 23, it can be seen that leakage current of PD-PWM, PD-PWM, and HB-PWM becoming higher with increased parasitic capacitance, which is determined by the characteristics of capacitance device. Fig. 23(a) and (b) shows that the leakage current trend of PD-PWM and PS-PWM are raising with dc-link voltage increasing, for the higher d*u*/d*t* of the switching frequency, which is attributed to the *LC* series leads to the increase of high-frequency components of parasitic capacitor voltage. And the leakage current shows a trend of first increasing and then decreasing with the increase resonance formed by parasitic capacitance and filtering inductance. The impedance of the leakage current loop is extremely small when the switching frequency approaches the resonant frequency. Thus, resonant frequencies should be considered when selecting switching frequencies and filters.

On the contrary, from Fig. 23(c), we can find the leakage current of HB-PWM will not be affected by switching frequency (f_s) and dc-link voltage. The reason is that the U_{SPCV} does not include switching components.

D. Efficiency Analysis

Fig. 24 shows the output voltage diagram of CHB inverter with three-module, the positive half cycle includes areas I, II, III, while the negative half cycle includes areas IV, V, VI. The

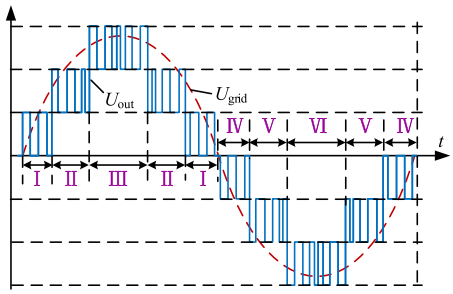

Fig. 24. Converter output voltage pattern.

TABLE VIII
CONDUCTION LOSSES BETWEEN CONVENTIONAL AND PROPOSED TOPOLOGIES

U_{out}	PD-PWM	PS-PWM	HB-PWM
0	3 Sw. and 3 D.	3 Sw. and 3 D.	5 Sw. and 1 D.
$\pm U_{PV}$	4 Sw. and 2 D.	4 Sw. and 2 D.	6 Sw.
$\pm 2U_{PV}$	5 Sw. and 1 D.	5 Sw. and 1 D.	5 Sw. and 1 D.
$\pm 3U_{PV}$	6 Sw.	6 Sw.	6 Sw.

Notes: Sw.–Switch, D.–Diode

TABLE IX
SWITCHING LOSSES AMONG CONVENTIONAL AND PROPOSED TOPOLOGIES

Region	mod.	Traditional modulation		Proposed method
		PD-PWM	PS-PWM	HB-PWM
I/IV	mod. 1	0	2 Sw. and 1 D.	2 Sw.
	mod. 2	0	2 Sw. and 1 D.	3 Sw. and 1 D.
	mod. 3	2 Sw. and 1 D.	2 Sw. and 1 D.	2 Sw.
II/V	mod. 1	0	2 Sw. and 1 D.	0
	mod. 2	2 Sw. and 1 D.	2 Sw. and 1 D.	3 Sw. and 1 D.
	mod. 3	0	2 Sw. and 1 D.	0
III/VI	mod. 1	2 Sw. and 1 D.	2 Sw. and 1 D.	0
	mod. 2	0	2 Sw. and 1 D.	3 Sw. and 1 D.
	mod. 3	0	2 Sw. and 1 D.	0

Notes: Sw.–Switch, D.–Diode, mod.–module

conduction loss and switching loss are key factors that affect the efficiency of converter. This article evaluates the overall efficiency of the proposed and conventional method (PD-PWM and PS-PWM) by analyzing the conduction loss and switching loss shown in Tables VIII and IX.

According to Table VIII, at the output voltage $U_{\rm out} = \pm 2U_{\rm PV}$, $U_{\rm out} = \pm 3U_{\rm PV}$, the amount of conduction losses of all methods is equal to each other. However, at the output voltage $U_{\rm out} = \pm 1U_{\rm PV}$, $U_{\rm out} = 0$, the amount of conduction losses of the proposed method is higher than that of the conventional method due to the addition of extra switches.

TABLE X
COMPARING THE PROPOSED METHOD WITH OTHER SOLUTIONS

Method	Type	No. of cascade module	No. of extra devices (IGBT, *L*, *C*, filter)	Exp.	Affe-cted by f_s	Volt. Str.	Curr. Str.	*Leak. curr.* (mA)	Efficie-ncies	Shortcomings
[25]	H	*n*	(2*C*+2CMV-filter) for each cell	Yes	Yes	U_{PV}	i_g	8.1	not report	**I.** Too many devices need to be added. **II.** Increased volume and weight. **III.** Filter is sensitive to switching frequency
[32]	H	*n*	*LCL*-filter for each module	Yes	Yes	U_{PV}	i_g	12	not report	
[22]	M	4	0	No	No	U_{PV}	i_g	24	not report	**I.** Unable to expand **II.** Unable be applied to odd modules
[28]	M	2	0	No	No	U_{PV}	i_g	15	98%	
[33]	H&M	2	(IGBT*1+*L**2 +*C**1) for each module	Yes	Yes	U_{PV}	i_g	14.2	98.2%	**I.** Too many devices need to be added. **II.** Inductance parameter matching is required **III.** Filter is sensitive to switching frequency
[34]	H&M	*n*	(IGBT*2+*L**2 +*C**1) for each module	Yes	Yes	U_{PV}	i_g	10.26	not report	
Proposed method	H&M	*n*	(IGBT*2) for OM-CHB	Yes	No	U_{PV}	i_g	3.3	98.1	Only applied to odd module.

Notes: H–Hardware, M–Modulation, H and M–Hardware and Modulation, fs–switching frequency, IGBT–Insulated gate bipolar transistor, Volt. Str.–Voltage stress, Curr. Str.–Current stress, Leak. curr.–leakage current, Exp.–Expandable, U_{PV}–the voltage of dc-link, i_g–the grid current.

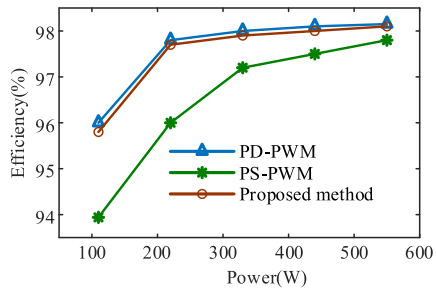

Fig. 25. Measured efficiency comparison curve.

As shown in Table IX, the switch status of module-1 and module-3 under proposed method are similar, which not switching in areas II/V and III/VI, making the proposed method have lower switching losses than traditional PS-PWM modulation. In addition, the number of switches of PD-PWM is less than proposed method at any areas. In brief, the switching losses of the proposed method is higher than PD-PWM while lower than PS-PWM.

Fig. 25 illustrates the experimental results for efficiency under different grid connected power of PD-PWM, PS-PWM, and proposed method. The experimental efficiencies of three methods at rated 550 W power are 98.15%, 97.6%, and 98.08% in succession. However, if traditional approach is utilized, a grid-side transformer must be used to avoid leakage current, which reduces system efficiency by 1% – 2%. In a word, proposed topology and its modulation have higher conversion efficiency than conventional methods.

The comparison of the proposed method with other methods are shown in Table X, which shows that the proposed topology just needs to add two small active switching devices, and cooperates with the proposed HB-PWM can ensure that the U_{SPCV} is free of any high-frequency components.

VI. CONCLUSION

In this article, a new topology and modulation strategy is proposed to reduce the leakage current for transformerless OM-CHB in PV systems, and its effectiveness was verified by theoretical analysis, simulation verifications, experimental tests. The proposed topology was implemented by only adding two power switches to middle module, and cooperate with the proposed modulation strategy can be eliminate the high-frequency components of the U_{SPCV} of OM-CHB completely, thus, leakage current gets suppressed. Compare to the most existing methods for suppress leakage current, the proposed method can be easily extended to any OM-CHB inverters, and the dc-link voltage and switching frequency have no influence on the proposed solution.

Despite all these features, this method has some limitations. First, the proposed method could be effective in reduction of the grid leakage current, however, cannot minimize the leakage current of each module. Second, the proposed method has excellent performance on leakage current suppression when the PV array light is balanced, but the local shadow occlusion is an inevitable problem in actual engineering situation. Therefore, further studies need to be explored.

REFERENCES

[1] J. Li et al., "How to make better use of intermittent and variable energy? A review of wind and photovoltaic power consumption in China," *Renewable Sustain. Energy Rev.*, vol. 137, 2021, Art. no. 110626, doi: 10.1016/j.rser.2020.110626.

[2] A. Fernandez-Guillamon, E. Gomez-Lazaro, E. Muljadi, and A. Molina-Garcia, "Power systems with high renewable energy sources: A review of inertia and frequency control strategies over time," *Renewable Sustain. Energy Rev.*, vol. 115, Nov. 2019, Art. no. 109369, doi: 10.1016/j.rser.2019.109369.

[3] C. Dhanamjayulu, P. Sanjeevikumar, and S. M. Muyeen, "A structural overview on transformer and transformer-less multi level inverters for renewable energy applications," *Energy Rep.*, vol. 8, pp. 10299–10333, Nov. 2022, doi: 10.1016/j.egyr.2022.07.166.

[4] K. Zeb et al., "A comprehensive review on inverter topologies and control strategies for grid connected photovoltaic system," *Renewable Sustain. Energy Rev.*, vol. 94, pp. 1120–1141, Oct. 2018, doi: 10.1016/j.rser.2018.06.053.
[5] W. Chen, X. Yang, W. Zhang, and X. Song, "Leakage current calculation for PV inverter system based on a parasitic capacitor model," *IEEE Trans. Power Electron.*, vol. 31, no. 12, pp. 8205–8217, Dec. 2016, doi: 10.1109/tpel.2016.2517740.
[6] M. F. Kibria, A. Elsanabary, K. S. Tey, M. Mubin, and S. Mekhilef, "A comparative review on single phase transformerless inverter topologies for grid-connected photovoltaic systems," *Energies*, vol. 16, no. 3, Feb. 2023, Art. no. 1363, doi: 10.3390/en16031363.
[7] H. Xiao and S. Xie, "Leakage current analytical model and application in single-phase transformerless photovoltaic grid-connected inverter," *IEEE Trans. Electromagn. Compat.*, vol. 52, no. 4, pp. 902–913, Nov. 2010, doi: 10.1109/temc.2010.2064169.
[8] *Automatic Disconnection Device Between a Generator and the Public Low-Voltage Grid*, DIN VDE V 0126-1-1, 2013.
[9] *Safety of Power Converters for use in Photovoltaic Power Systems - Part 2: Particular Requirements for Inverters*, IEC 62109-2, 2012.
[10] H. Li, Y. B. Zeng, B. Zhang, T. Q. Zheng, R. X. Hao, and Z. Yang, "An improved H5 topology with low common-mode current for transformerless PV grid-connected inverter," *IEEE Trans. Power Electron.*, vol. 34, no. 2, pp. 1254–1265, Feb. 2019, doi: 10.1109/tpel.2018.2833144.
[11] W. Yu, J.-S. Lai, H. Qian, and C. Hutchens, "High-efficiency MOSFET inverter with H6-type configuration for photovoltaic nonisolated AC-module applications," *IEEE Trans. Power Electron.*, vol. 26, no. 4, pp. 1253–1260, Apr. 2011, doi: 10.1109/tpel.2010.2071402.
[12] T. K. S. Freddy, N. A. Rahim, W.-P. Hew, and H. S. Che, "Modulation techniques to reduce leakage current in three-phase transformerless H7 photovoltaic inverter," *IEEE Trans. Ind. Electron.*, vol. 62, no. 1, pp. 322–331, Jan. 2015, doi: 10.1109/tie.2014.2327585.
[13] A. Hota and V. Agarwal, "Novel three-phase H10 inverter topology with zero or constant common-mode voltage for three-phase induction motor drive applications," *IEEE Trans. Ind. Electron.*, vol. 69, no. 7, pp. 7522–7525, Jul. 2022, doi: 10.1109/tie.2021.3097656.
[14] T. Yu, W. Wan, and S. Duan, "A modulation method to eliminate leakage current and balance neutral-point voltage for three-level inverters in photovoltaic systems," *IEEE Trans. Ind. Electron.*, vol. 70, no. 2, pp. 1635–1645, Feb. 2023, doi: 10.1109/tie.2022.3161809.
[15] W. Jiang et al., "A novel virtual space vector modulation with reduced common-mode voltage and eliminated neutral point voltage oscillation for neutral point clamped three-level inverter," *IEEE Trans. Ind. Electron.*, vol. 67, no. 2, pp. 884–894, Feb. 2020, doi: 10.1109/tie.2019.2899564.
[16] X. Guo, Y. Yang, and T. Zhu, "ESI: A novel three-phase inverter with leakage current attenuation for transformerless PV systems," *IEEE Trans. Ind. Electron.*, vol. 65, no. 4, pp. 2967–2974, Apr. 2018, doi: 10.1109/tie.2017.2757916.
[17] S. Bhattacharya, D. Mascarella, G. Joos, J.-M. Cyr, and J. Xu, "A dual three-level T-NPC inverter for high-power traction applications," *IEEE J. Emerg. Sel. Topics Power Electron.*, vol. 4, no. 2, pp. 668–678, Jun. 2016, doi: 10.1109/jestpe.2016.2517819.
[18] X. Q. Guo et al., "Overview of recent advanced topologies for transformerless dual-grounded inverters," *IEEE Trans. Power Electron.*, vol. 37, no. 10, pp. 12679–12704, Oct. 2022, doi: 10.1109/TPEL.2022.3170931.
[19] A. Kumar and P. Sensarma, "A four-switch single-stage single-phase buck-boost inverter," *IEEE Trans. Power Electron.*, vol. 32, no. 7, pp. 5282–5292, Jul. 2017, doi: 10.1109/TPEL.2016.2605150.
[20] F. Peng, G. H. Zhou, N. M. Xu, and S. Gao, "Zero leakage current single-phase quasi-single-stage transformerless PV inverter with unipolar SPWM," *IEEE Trans. Power Electron.*, vol. 37, no. 11, pp. 13755–13766, Nov. 2022, doi: 10.1109/TPEL.2022.3180287.
[21] N. Vazquez, J. Vazquez, J. Vaquero, C. Hernandez, E. Vazquez, and R. Osorio, "Integrating two stages as a common-mode transformerless photovoltaic converter," *IEEE Trans. Ind. Electron.*, vol. 64, no. 9, pp. 7498–7507, Sep. 2017, doi: 10.1109/TIE.2017.2682014.
[22] I. Gunsal, D. A. Stone, and M. P. Foster, "Suppressing leakage current for cascaded H-bridge inverters in renewable energy and storage systems," *IEEE Trans. Ind. Electron.*, vol. 68, no. 11, pp. 11035–11043, Nov. 2021, doi: 10.1109/tie.2020.3031524.
[23] H. Iman-Eini, S. Bacha, and D. Frey, "Improved control algorithm for grid-connected cascaded H-bridge photovoltaic inverters under asymmetric operating conditions," *IET Power Electron.*, vol. 11, no. 3, pp. 407–415, Mar. 2018, doi: 10.1049/iet-pel.2016.0983.
[24] A. A. Valdez-Fernandez, G. Escobar, D. U. Campos-Delgado, and M. E. Hernandez-Ruiz, "Model-based control strategy for the three-phase n-level CHB multilevel converter," *Int. J. Elect. Power Energy Syst.*, vol. 147, May 2023, Art. no. 108883, doi: 10.1016/j.ijepes.2022.108883.
[25] Y. Zhou and H. Li, "Analysis and suppression of leakage current in cascaded-multilevel-inverter-based PV systems," *IEEE Trans. Power Electron.*, vol. 29, no. 10, pp. 5265–5277, Oct. 2014, doi: 101109/TPEL20132289939.
[26] K. Chen et al., "Cascaded iH6 multilevel inverter with leakage current reduction for transformerless grid-connected photovoltaic system," in *Proc. IEEE 12th Int. Conf. Power Electron. Drive Syst.*, 2017, pp. 613–617.
[27] F. K. Moghaddam and H. Iman-Eini, "Reliable simple method for suppression of leakage current in grid-connected CHB inverters," *IET Power Electron.*, vol. 11, no. 13, pp. 2170–2177, Nov. 2018, doi: 10.1049/iet-pel.2018.5526.
[28] F. Wang, Z. Li, H. T. Do, and D. Zhang, "A modified phase disposition pulse width modulation to suppress the leakage current for the transformerless cascaded H-bridge inverters," *IEEE Trans. Ind. Electron.*, vol. 65, no. 2, pp. 1281–1289, Feb. 2018, doi: 10.1109/tie.2017.2733488.
[29] G. Vazquez, P. R. Martinez-Rodriguez, G. Escobar, J. M. Sosa, and R. Martinez-Mendez, "A PWM method for single-phase cascade multilevel inverters to reduce leakage ground current in transformerless PV systems," *Int. Trans. Elect. Energy Syst.*, vol. 26, no. 11, pp. 2353–2369, Nov. 2016, doi: 10.1002/etep.2208.
[30] R. Selvamuthukumaran, A. Garg, and R. Gupta, "Hybrid multicarrier modulation to reduce leakage current in a transformerless cascaded multilevel inverter for photovoltaic systems," *IEEE Trans. Power Electron.*, vol. 30, no. 4, pp. 1779–1783, Apr. 2015, doi: 10.1109/tpel.2014.2345501.
[31] F. Wang, S. Y., L. Yang, W. Mao, and X. Zhang, Modulation Method for Suppressing Leakage Current in H-Bridge Cascaded Inverters. China. 2018, CN 105610343 A.
[32] M. Shahabadini and H. Iman-Eini, "Leakage current suppression in multilevel cascaded h-bridge based photovoltaic inverters," *IEEE Trans. Power Electron.*, vol. 36, no. 12, pp. 13754–13762, Dec. 2021, doi: 10.1109/tpel.2021.3084699.
[33] X. Guo and X. Jia, "Hardware-based cascaded topology and modulation strategy with leakage current reduction for transformerless PV systems," *IEEE Trans. Ind. Electron.*, vol. 63, no. 12, pp. 7823–7832, Dec. 2016, doi: 10.1109/tie.2016.2607163.
[34] M. Shahabadini, N. Moeini, M. Bahrami-Fard, and H. Iman-Eini, "HERIC-based cascaded H-bridge inverter for leakage current suppression in PV systems," *IEEE Trans. Power Electron.*, vol. 38, no. 3, pp. 4005–4014, Mar. 2023, doi: 10.1109/tpel.2022.3218634.
[35] W. Mao et al., "Research on power equalization of three-phase cascaded H-bridge photovoltaic inverter based on the combination of hybrid modulation strategy and zero-sequence injection methods," *IEEE Trans. Ind. Electron.*, vol. 67, no. 11, pp. 9337–9347, Nov. 2020, doi: 10.1109/TIE.2019.2955420.

Pengcheng Zhao (Student Member, IEEE) was born in Sichuan, China, in 1994. He received the B.S. degree in electrical engineering and automation and the M.S. degree in control engineering from Southwest Petroleum University, Chengdu, China, in 2018 and 2021, respectively. He is currently working toward the Ph.D. degree in electrical engineering with Southwest Jiaotong University (SWJTU), Chengdu, China.

His research interests include multilevel converters, photovoltaic grid-connected inverter, and renewable energy power conversion systems.

Xiaoqiong He (Member, IEEE) received the B.S., M.S., and D.Eng. degrees in electrical engineering from Southwest Jiaotong University, Chengdu, China, in 1998, 2003, and 2013, respectively.

She was a visiting scholar for one year in Nanyang Technological University. Her research interests include power electronic transformer and its application, rail transit electrification and automation, fault diagnosis and system reconstruction of converter, and new semiconductor devices (SiC, GaN) application research.

Dr. He was the recipient of the first prize of Sichuan Provincial Technology Invention, the first prize of China Railway Society Science and Technology, and one first prize of Sichuan Provincial Teaching Achievement.

She was general chair of IEEE ICIEA 2022 and the distinguished lecturer speaker of IECON 2023.

Yikai Wang was born in Sichuan, China, in 1999. He received the B.S. degree in electronic information engineering in 2021 from Southwest Jiaotong University, Chengdu, China, where he is currently working toward the M.S. degree in electronic information.

His research interests include the stability analysis of dc microgrid, solar system control, and power electronics converters.

Chenghao Qiu was born in Liaoning, China, in 1999. He received the B.S. degree from Dalian Jiaotong University, Dalian, China, in 2021, and is currently working toward the M.S. degree with Southwest Jiaotong University, Chengdu, China, all in electrical engineering.

His research interests include cascaded converters, the control of pulse width modulation rectifier, and new energy power generation.

Pengcheng Han (Student Member, IEEE) was born in Henan, China. He received the Bachelor of Science and Doctor of Engineering degrees in electrical engineering from Southwest Jiaotong University, Chengdu, China, in 2015 and 2022, respectively.

His research interests include multilevel converters and control applications to power electronic converters.